



# Robot odor source localization in indoor environments based on gradient adaptive extremum seeking search



Meh Jabeen <sup>a,b</sup>, Qing-Hao Meng <sup>a</sup>, Tao Jing <sup>a</sup>, Hui-Rang Hou <sup>a,\*</sup>

<sup>a</sup> Tianjin Key Laboratory of Process Measurement and Control, Institute of Robotics and Autonomous Systems, School of Electrical and Information Engineering, Tianjin University, Tianjin, 300072, PR China

<sup>b</sup> Department of Software Engineering, The University of Lahore, Lahore, 54590, Pakistan

## ARTICLE INFO

### Keywords:

Odor source localization  
Extremum seeking control  
Three-point gradient estimation  
Adaptive feedback gain  
Indoor environment

## ABSTRACT

When toxic or harmful chemicals or pollutants leak, it is of great significance to determine the leakage source(s) in a timely and autonomous manner to reduce casualties and property losses. This study focuses on the problem of robot-based odor source localization (OSL) in unknown indoor environments from a control perspective. A model-free gradient adaptive extremum seeking control (GA-ESC) algorithm was proposed to improve the searching efficiency and success rate of OSL. The GA-ESC algorithm plans the OSL through a controller, which estimates the gradient of the odor plume concentration, and guides the robot to approach the odor source according to the estimated gradient. A novel three-point gradient estimation method was proposed to obtain a more stable odor field gradient based on two historical points and one current point, where an adaptive feedback gain was applied to link the estimated gradient and the output control quantities. Subsequently, the perturbation amplitude adjustment (PAA) strategy was introduced to enhance the global searching ability. When compared to the traditional extremum seeking control (ESC), our algorithm outperforms it in terms of success rate and average searching time. Moreover, the performance of the proposed algorithm was validated through simulations by utilizing three different dispersion models. The real-robot experiments were also carried out in indoor environments. The results demonstrate the significance of the proposed control-based OSL algorithm in unknown indoor environments.

## 1. Introduction

The indoor environment is considerably significant to human health and safety. However, the buildings such as industrial workshops, laboratories, offices, and residences suffer from the safety hazards of toxic, harmful, flammable, or explosive gas leakage. Once relevant dangerous accidents occur, e.g., the "8.4" explosion in Beirut port, Lebanon, in 2020 and the "2.26" flash explosion in Xianlong, Hubei, China in 2021, they will cause irreparable damage to life, property, and the environment [1, 2]. To this end, early and accurately detecting and tracing the gas plumes [3], and effectively locating the gas leakage sources [4] will be instrumental in radically reducing the occurrence of such dangerous situations, while improving indoor air quality across the board to meet expectations for a safe, healthy and comfortable building environment.

Generally, odor source localization (OSL) can be divided into sensor network-based static localization and robot-based active olfaction. The latter, i.e., robot OSL, refers to the research of localizing one or more

volatile chemical sources in an airflow or water environment based on one or more mobile robots equipped with gas sensors, which could significantly reduce the detrimental impact on humans in hazardous gas leakage situations [5–7]. From the perspective of basic ideas applied, the existing OSL algorithms could be roughly classified into three categories: reactive algorithms, probabilistic algorithms, and the optimization algorithms.

The reactive algorithms explicitly couple odor perception to robot action, containing two subcategories: the gradient-based algorithms and the bio-inspired algorithms. The gradient-based algorithms make use of the measured odor gradient and drive the robot towards the ascending direction of the gradient, which is more applicable in a diffusion-dominated environment [8]. The bio-inspired algorithms are inspired by the olfactory behaviors of some organisms, such as lobster [9], silk-worm moth [10], and dung beetles [11], which could be interpreted as finite state machines with simple reactive rules for each of the inputs of each state. Bio-inspired algorithms are thoroughly assessed in Ref. [3]

\* Corresponding author.

E-mail address: [houuirang@tju.edu.cn](mailto:houuirang@tju.edu.cn) (H.-R. Hou).

for indoor plumes. To this end, these algorithms are computationally efficient [3,12].

The probabilistic algorithms model a belief on the source location in the context of a probability distribution obtained from observations made by robots in the environment [13]. For each observation, the belief is updated using Bayesian estimation. This process continues until the probability distribution is reduced to a Dirac function. Particle filter-based algorithm [14,15], Entrotaxis [16], and Infotaxis [17] are some of the primary examples of this category. However, these algorithms have a high computational cost and require accurate localization of the sampling points, which is difficult for some old hardware platforms. Since the related technologies have progressed rapidly in recent decades, these algorithms are no longer a colossal burden [4].

The optimization algorithms regard the robot OSL task as an optimization problem, trying to find the best solution (i.e., the odor source location) from all the feasible solutions (i.e., the searching area) through heuristic means. The optimization problem is solved based on some heuristic searching methods like particle swarm optimization (PSO) algorithms [18]. The optimization algorithms are usually based on multi-robots [19,20]. Improved optimization algorithms are recently studied in Ref. [19] using multi-robots in an indoor ventilated environment. Multi-robots could have obvious advantages over single robots in terms of efficiency and robustness.

As mentioned above, significant progress has been made in OSL as well as the related algorithms. However, most of the OSL algorithms i.e., the reactive, probabilistic, and the optimization algorithms do not often hold true in GPS-denied unknown environments (e.g., the deep sea, underground, or even indoor environments) and easily trapped in the local optimum, where the robot relies on sensor information [22], due to either their complex models or ignoring the dynamics of the robots. In contrast, the control-based source-searching algorithms take into consideration the dynamics of the robot. For the first time, the extremum seeking control (ESC) was employed for source seeking by Zhang et al. [23]. ESC estimates the extremum (maximum/minimum) of the gradient information using averaging technique via singular perturbation signal, which is the combination of the sensor signal and control signal (e.g., sinusoidal signal) [23]. The goal of ESC is to find the optimal setpoint (extremum) and drive the robot there along the estimated gradient. The robots using ESC don't need to know their location to find the extremum point (i.e., the odor source location). ESC-based source seeking with non-holonomic agents is addressed in Refs. [24–29]. In Refs. [30,31], a quick review of the ESC from the source-seeking perspective is provided.

The ESC is naturally a “gradient search” method and can be used to estimate the gradient of an unknown reference-to-output mapping. The existing ESC is generally employed for scalar signal source seeking, such as thermal, radar, and electromagnetic sources. However, in a real environment, the gradient information of certain signals, such as a chemical source (odor source) is complex (i.e., having multiple local extrema) owing to the impact of wind turbulence. Moreover, the gradient estimation in the traditional ESC problem is based on the fixed feedback gain method. It might be only applicable for a steady distribution signal (e.g., light source or magnetic field). But in the turbulence-dominated environment, the gradient of odor concentration is unsteady, noisy, and the gradient information of the odor dispersion model is unstable. Consequently, it is not surprising that the traditional ESC could converge to one of the local extrema [32] if it exists. To find the global extremum, the user of ESC often observes that by tuning the parameters of the traditional ESC, it is possible to pass the local extrema and converge to the global extremum [21,33]. Motivated by the above observations, we present the novel gradient adaptive extremum seeking control (GA-ESC) for OSL, having an ability to tune the parameters of the traditional extremum seeking control adaptively. The proposed algorithm can adjust to the external impacts of the signal due to its configurable parameters, and the gradient estimation method allows the robots to explore additional gradient points (i.e., three points), making

them to swiftly escape the local extremum. The main contributions of this study are summarized as follows.

- A completely new paradigm, that is, to address the OSL problem from the perspective of control, was proposed for the first time.
- The proposed GA-ESC method can control the robot approach the odor source owing to its online gradient estimation method without relying on the robot's absolute position and distribution of the signal field, as well as without using any airflow sensors. (Please see the ‘Supplementary information’ for the stability analysis of the GA-ESC algorithm.)
- The perturbation amplitude adjustment (PAA) strategy [21,33] has been introduced into GA-ESC for further improving its global searching ability. The traditional ESC extremizes the output by employing a perturbation signal to extract gradient information from the reference-to-output map, which may lead the output to converge to a local extremum rather than the global extremum in the presence of multiple extrema. To improve the global searching ability, we introduced the PAA strategy into a GA-ESC, named GA-ESC with PAA.
- The OSL performance of the proposed GA-ESC method has been validated via simulations and experiments in an indoor unknown environment, where the simulation uses three dispersion models that reflect three various environmental conditions (i.e., indoor environment without ventilation, environment with steady and strong wind, and simulated environment equivalent to real-world).

The remainder of this paper is organized as follows. Section 2 presents the odor dispersion models involved in this study. Section 3 introduces the principle of traditional ESC, GA-ESC, and GA-ESC with PAA including the procedure of OSL using the proposed algorithm. Simulations and real-robot experiments are detailed in section 4 and section 5, respectively, followed by conclusions.

## 2. Odor dispersion models

Odor diffusion simulations in indoor environment were performed based on three models: the symmetric quadratic model, the advection-diffusion model [34], and the filament-based plume model [35], to evaluate the efficiency of the proposed algorithm.

### 2.1. Symmetric quadratic model

For the symmetric quadratic model, the odor concentration distributes smoothly in a quadratic manner as the distance to the source increases. This model is associated with the diffusion-dominated environment (e.g., an indoor environment without ventilation). The symmetric quadratic model is expressed as:

$$f(x_i, y_i) = f^* - \frac{(x_i - x^*)^2 + (y_i - y^*)^2}{k}, \quad (1)$$

where  $f(x_i, y_i)$  is the odor concentration at the point  $(x_i, y_i)$ ,  $f^*$  is the extremum value of odor concentration,  $(x^*, y^*)$  symbolizes the extrema (i.e., the source location), and  $k$  denotes the diffusion coefficient.

### 2.2. Advection-diffusion model

The advection-diffusion model describes the environment with steady and strong wind. Considering an environment with a one-direction wind field where the time-averaged wind speed is constant and the wind turbulence is isotropic and homogeneous, the time-averaged gas distribution from a point source can be expressed as:

$$f(x_i, y_i) = \frac{q}{2\pi k} \frac{1}{d} \exp \left[ -\frac{U}{2k} (d - (x_i - x^*)) \right], \quad (2)$$

where  $q$  stands for the gas release rate,  $U$  represents the wind speed, and  $d = \sqrt{(x_i - x^*)^2 + (y_i - y^*)^2}$ .

### 2.3. Filament-based model

Odor plume in the real environment is intermittent, meandering, and time-varying [35]. To obtain an odor dispersion model closer to the real odor characteristics, the filament-based model is adopted. The filament-based model is computationally efficient and designed to simulate the short-term signature as well as the long-term exposure statistics of a chemical plume evolving in a turbulent flow [35]. It does not rely on the mathematical plume model but is based on different physical phenomena that occur during plume dispersion.

The odor plume can be presented as a sequence of puffs in the filament-based model, as shown in Fig. 1. Each puff is composed of many filaments, and each filament is modeled as a 3D normal distribution of molecules. The odor dispersion process is dominated by turbulence and molecular diffusion, which involves a wide range of eddies. Eddies of different sizes have different effects on the puff flow as follows [35].

- Eddies smaller than the puff mix the puff components and cause a slight puff motion or growth (diffusion  $U_d$ ).
- Eddies on the order of the puff's scale cause substantial puff growth and distortion (intermediate-range scales  $U_m$ ).
- Eddies larger than the puff transport the puff as a whole, causing an advective flow over the filaments (advection  $U_a$ ).

Considering molecular diffusion and advection, the velocity of the  $i^{th}$  filament can be calculated as follows:

$$U_{fila-i} = U_a + U_{d-i}, \quad (3)$$

where,  $U_{fila-i}$  stands for the velocity of the  $i^{th}$  filament's center,  $U_a$  is the advection velocity caused by the big eddies advection effect, and  $U_{d-i}$  denotes the diffusion velocity of the filament with respect to the plume centerline. We obtained the advection velocity through the CFD software, and the diffusion velocity is generated according to a normal distribution.

After obtaining the distribution of the filament, the odor concentration distribution can be further calculated. For a given position  $X$  at any time  $t$ , the concentration distribution of the  $i^{th}$  filament can be expressed as:

$$C_i(X, t) = \frac{Q}{\sqrt{8\pi^2 R_i^3(t)}} \exp\left(\frac{-r_i^3(t)}{R_i^2(t)}\right) \frac{\text{molecules}}{\text{cm}^2 \text{filament}}, \quad (4)$$

where,  $Q$  represents the amount of molecules per filament,  $R_i$  is a parameter controlling the size of the  $i^{th}$  filament,  $r_i(t)$  is the Euclidean distance between the position  $X$  and the  $i^{th}$  filament. The overall concentration at the position  $X$  at the time  $t$  is the sum of the concentrations at that position contributed by each filament, is expressed as:

$$C(X, t) = \sum_{i=1}^N C_i(X, t) \frac{\text{molecules}}{\text{cm}^2}. \quad (5)$$

### 3. The GA-ESC methods

In this section, we first describe the non-holonomic unicycle robot model. Then we briefly state the basic ESC principle for source seeking and present our GA-ESC and GA-ESC with PAA approaches for the OSL task. Additionally, the procedure of the OSL using the proposed algorithm is covered in this section.

#### 3.1. The robot model

We consider a non-holonomic unicycle robot model with the sensor mounted in the middle. According to Fig. 2, the kinematic of the robot model is given as:

$$\begin{cases} \dot{x}_c = v \cos \theta \\ \dot{y}_c = v \sin \theta \\ \dot{\theta} = \Omega \end{cases}, \quad (6)$$

where,  $(x_c, y_c)$  represents the robot's position,  $\theta$  denotes the orientation,  $v$  and  $\Omega$  are forward velocity and the angular velocity, respectively.

The task of the robot is to localize the source that emits a kind of measurable gas signal. The distribution of the signal field is unknown; however, it is assumed that the signal intensity is maximal at the source location and decays away from it [22,32]. A robot uses the measured signal at the sensor's location as the input of the control loop. Without loss of generality, we use the control strategy of tuning the forward velocity while keeping the angular velocity input constant to accomplish

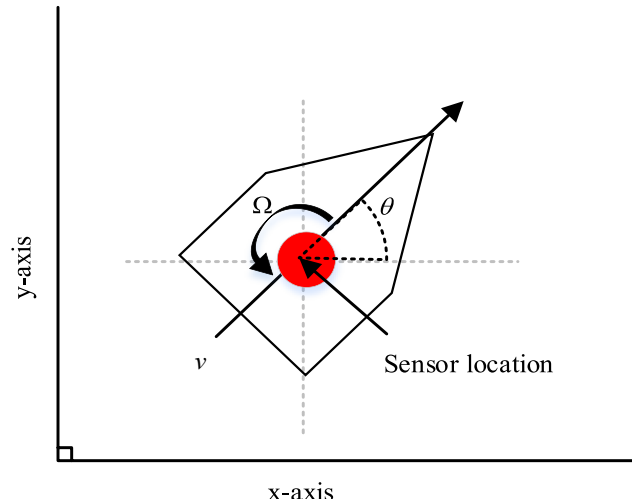


Fig. 2. Non-holonomic unicycle robot model.

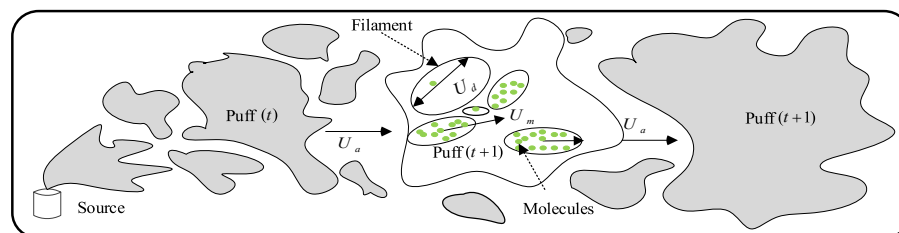


Fig. 1. Representation of puffs using the filament-based model. Advection and diffusion have an impact on the plume's puffs. To develop a corresponding plume simulation model, the velocity vector will be decomposed into three components:  $U_a$ ,  $U_m$ , and  $U_d$  [36].

the task.

### 3.2. The basic theory of ESC for source seeking

The ESC allows solving the optimization as a control problem, and its main objective is to find the extremum value of an unknown function  $J$ . The block diagram of ESC [22] is shown in Fig. 3. The nonlinear map represents the distribution of the signal (i.e., plume concentration distribution) being tracked by the robot. We assume that a nonlinear map (objective function)  $J = f(x_c, y_c)$  has a global optimum value  $f^*$  at  $(x^*, y^*)$  [22]. The ESC drives the robot toward the extremum  $f^*$  without employing any prior knowledge of the source of dispersion or the robot's position, only with the measurement of the output  $J$  (objective function). The ESC contains the following stages to optimize the objective function [30].

- Modulation – The value of input  $v$  (forward velocity) is perturbed using a sinusoidal signal  $a\omega \sin(\omega t)$  (where  $a$  and  $\omega$  are the amplitude and frequency of the signal, respectively) to estimate the gradient of the signal.
- System response – As for the controller, ESC inputs  $v$  (obtained from modulation) and  $\Omega$  (constant) to the robot model, and outputs  $(x_c, y_c)$  are fed into the objective function  $J$ . Hence, the input causes a corresponding change in the measurement of  $J$ .
- Demodulation – The output of  $J$  passes through the simple high-pass filter  $s/s + h$  (where,  $s$  denotes the Laplace variable and  $h$  stands for filter frequency), the output of the high-pass filter is then demodulated (multiplied) by the sinusoidal signal with the same frequency as the modulation signal, resulting in the signal  $\xi$ , where  $\xi = (s/s + h)a \sin(\omega t)$ .
- Feedback – the demodulated signal is integrated into the best guess  $\hat{v}(\hat{v} = c\xi)$  to optimize the input  $v$ . The feed gain  $c$  parameter determines how the robot responds to the signal field.

Based on the diagram in Fig. 3, the basic control law is described as:

$$v = a\omega \sin(\omega t) + c\xi, \quad (7)$$

where,  $a, \omega$  are positive design parameters.

### 3.3. Gradient-adaptive ESC (GA-ESC)

The traditional ESC performs well in diffusive-dominated environments, such as non-ventilated indoor or underground environments. However, as stated above, due to the intermittent nature of the gas dispersion, there might possess multiple local concentration maxima, so the traditional ESC may not be applicable for locating odor sources in complex environments (e.g., ventilated indoor environments with

steady/unsteady wind speed, or outdoor airflow environments). To address this problem, the GA-ESC, which estimates the gradient of the odor source by the three-point method, is proposed, as shown in Fig. 4 (the red dotted box), and the feedback gain  $c$  is adjusted according to the estimated gradient. Assume that  $(x_1, y_1)$  and  $(x_2, y_2)$  are two historical points related to the current point  $(x_0, y_0)$ .  $z_1$  and  $z_2$  are used to represent the strength of the signal at the points  $(x_1, y_1)$  and  $(x_2, y_2)$ , respectively. Thus, the vectors  $(x_1, y_1, z_1)$  and  $(x_2, y_2, z_1)$  are obtained, the estimated gradient vector is described as follows:

$$\nabla = \left( \frac{-A}{\sqrt{A^2 + B^2}}, \frac{-B}{\sqrt{A^2 + B^2}}, \sqrt{A^2 + B^2} \right). \quad (8)$$

In the gradient vector, the first two terms are the direction of the estimated gradient (coordinates of the vector), while the last term is the magnitude of the estimated gradient vector denoted by  $\hat{\Delta}$ , and

$$A = \frac{y_1 z_2 - y_2 z_1}{x_1 y_2 - x_2 y_1}, B = \frac{x_2 z_1 - x_1 z_2}{x_1 y_2 - x_2 y_1}. \quad (9)$$

The feedback gain  $c$  is a constant in the case of traditional ESC (Eq. (7)). However, in the GA-ESC algorithm, feedback gain  $c$  is automatically adjusted according to the magnitude of the estimated gradient vector as follows:

$$c = M/G(\hat{\Delta}), \quad (10)$$

where  $M$  is a constant but not necessarily zero, which determines the overall convergence rate,  $G(\cdot)$  represents a low-pass filter used to avoid an excessive increase in  $c$  value (tends to overshoot and instability). Hence, the control law for GA-ESC can be expressed as:

$$v = a\omega \sin(\omega t) + (M/G(\hat{\Delta}))\xi. \quad (11)$$

To estimate the gradient vector, only the relative position and gas concentration information of the nearest two historical points to the current point are required, and the relative position information can be obtained by the robot dead reckoning [37] but is unaffected by the cumulative error of dead reckoning. The gradient calculation method maintains the benefits of traditional ESC, which requires only signal strength and speed information and does not require a complex positioning system.

### 3.4. GA-ESC with perturbation amplitude adjustment (GA-ESC with PAA)

We assume that odor concentration is higher and unstable near the source and decreases as the distance from the source increases. In airflow environments, the dispersed odor might have an extreme concentration in multiple local locations. As a local optimizer [26], the traditional ESC could not efficiently find the odor source in real airflow

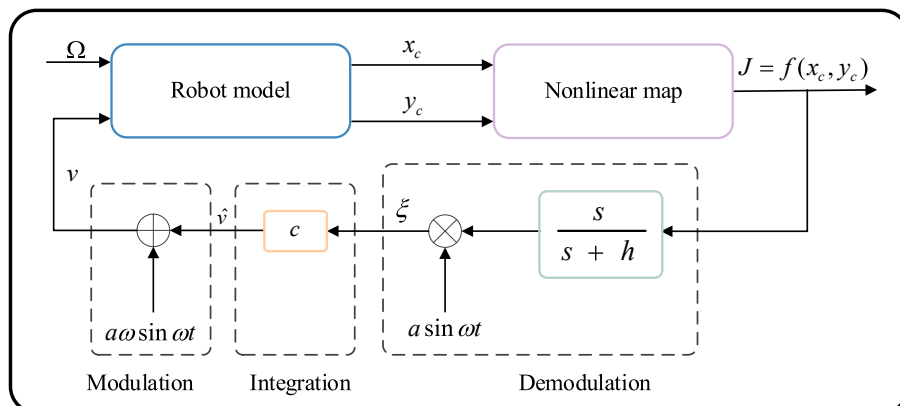


**Fig. 3.** Block diagram of ESC [22].

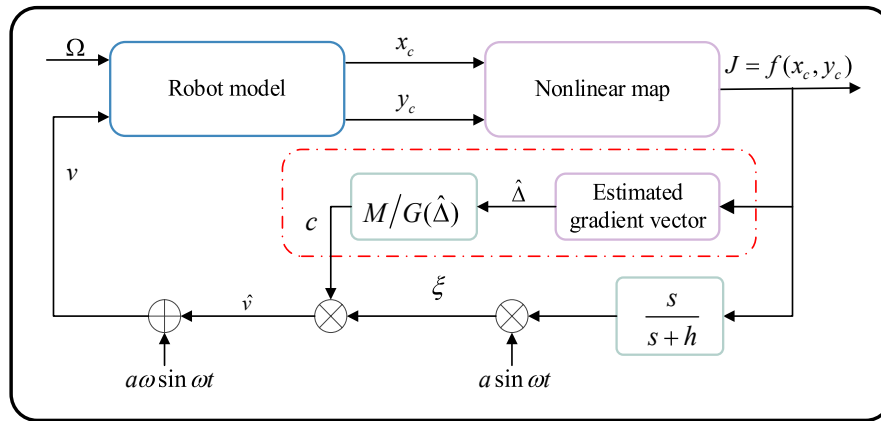


Fig. 4. Block diagram of GA-ESC.

environments. To enhance global searching ability, the concept of PAA has been added to the GA-ESC. We employ the larger perturbation signal and explore more gradient information to move toward the optimum point, and the larger perturbation amplitude leads to escape from the local optimum. The amplitude of the perturbation signal gradually decreases as the robot approaches the source. A smaller amplitude value reduces the influence of the larger perturbation signal close to the source and stabilizes the searching process [21]. The architecture of the GA-ESC with PAA is shown in Fig. 5 (the gray dotted box), where the PAA [33] is expressed as follows:

$$a = -\varepsilon \delta a, a(0) = a_0 > 0, \quad (12)$$

where,  $a_0$  represents the initial value of the perturbation amplitude,  $\varepsilon$ , and  $a_0$  are to be selected based on problem at hand and left to the choice of the designer. The feedback gain varies based on the magnitude of the estimated gradient and the amplitude of the perturbation signal and is denoted as:

$$c = M / (G(\hat{\Delta}) * a). \quad (13)$$

Furthermore, the control law for GA-ESC with PAA can be represented as follows:

$$v = a\omega \sin(\omega t) + [M / (G(\Delta) * a)]\xi. \quad (14)$$

### 3.5. Odor source localization procedure

The OSL procedure using GA-ESC/GA-ESC with PAA/traditional ESC algorithm includes the following steps (Fig. 6).

- Step 1: All the parameters of the algorithm and odor dispersion model are initialized.
- Step 2: The robot model employs the random walk strategy to depart from the starting point and to find the plume.
- Step 3: The counter is initiated as soon as the robot model locates the plume.
- Step 4: If the counter is less than one, the robot confirms the detection of the plume.
- Step 5: If the robot is out of the plume, jump to step 2, otherwise goes to step 6.
- Step 6: The robot starts tracking the plume via GA-ESC/GA-ESC with PAA/traditional ESC algorithm.
- Step 7: The simulation time counting (i.e., dis\_count) is started, and the extremum value is checked in every dis\_count. If the dis\_count is less than the specified period of time (e.g., 900 s), and the extremum value is detected, the counter is incremented, and the procedure is declared successful; otherwise, step 4 is repeated. The procedure is deemed unsuccessful if the dis\_count is higher than the specified time limit and the extremum value could not be located.

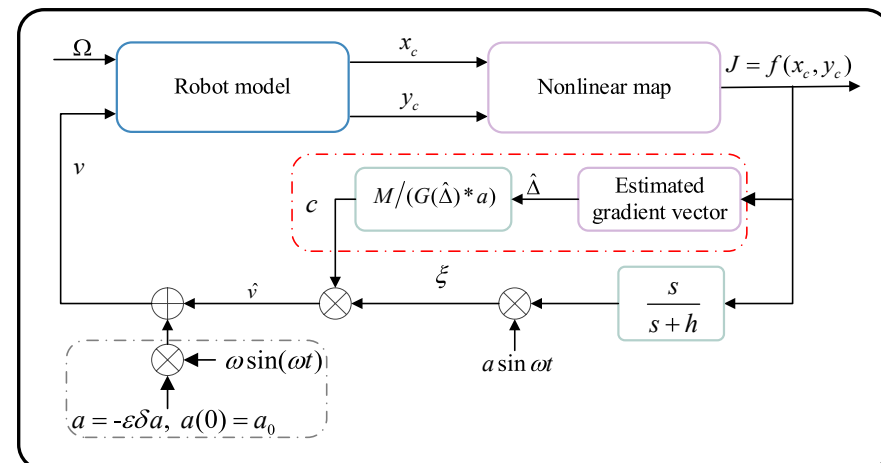
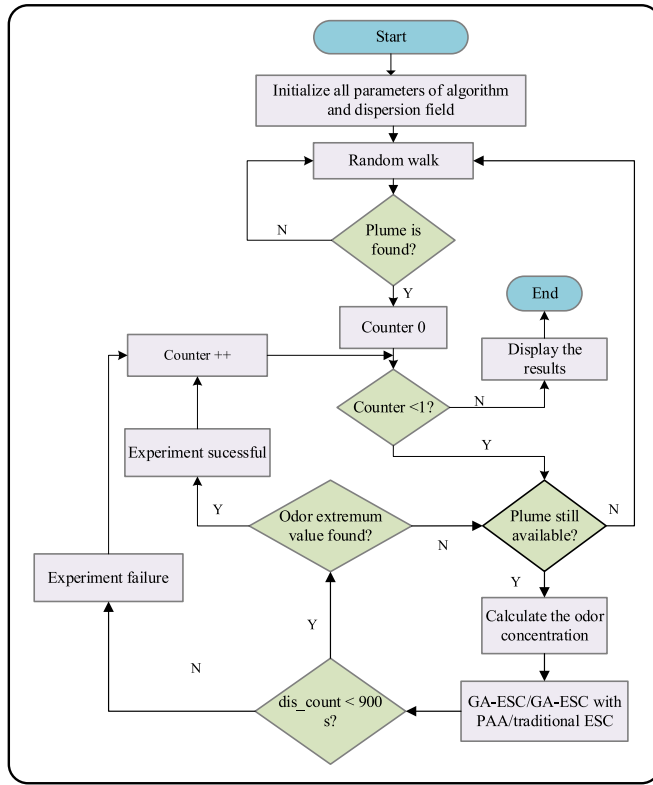


Fig. 5. Architecture of the GA-ESC with PAA.



**Fig. 6.** Procedure of the odor source localization using ESC methods.

#### 4. Simulations in an indoor environment

This section presents the simulations of the GA-ESC algorithm and the GA-ESC with PAA based on the three odor dispersion models. Simulations based on the symmetric quadratic model and the advection-diffusion model were conducted in MATLAB, and the results were compared with those using the traditional ESC algorithm. The filament-based plume dispersion model was implemented in the form of an integrated robot OSL simulator based on Visual C++. The flow chart of the simulator is shown in Fig. 7. The simulator mainly included the wind field simulation and the plume simulation. The environment wind was made up of the advection wind and the fluctuating wind. The advection wind was generated by FLUENT offline [15], while the fluctuation wind was obtained through real wind measurement. The plume model was then used as a signal field of proposed algorithms.

As far as the computational complexity is concerned, the proposed technique is computationally less expensive. The complexity of the proposed algorithm is  $O(n)$ , if the running time  $T(n)$  of the algorithm is defined as the worst-case running time over all instances of size  $n$ .

#### 4.1. Simulation in the symmetric quadratic model

The concentration distribution of the symmetric quadratic model is described in Eq. (1). The parameters of the dispersion model were chosen as the target source at  $(0, 0)$  m,  $f^* = 1$ , and  $k = 10$ . The parameters of the traditional ESC algorithm, the GA-ESC algorithm, and the GA-ESC with PAA are shown in Table 1.

Fig. 8 shows an example of each algorithm's results (trajectories) in the symmetric quadratic model. Fig. 8(a) illustrates the robot trajectory using the traditional ESC with  $c = 4$ . The robot starts at  $(0.5, 3)$  m by probing around the star pattern (The constant angular velocity ( $\Omega = \omega/5$ ) formed the star pattern in trajectory) to climb the gradient of the nonlinear map and converge gradually as it approaches the source. The GA-ESC searching trajectory is shown in Fig. 8(b), where the robot approaches the odor source consistently. The searching trajectory of the GA-ESC with PAA in Fig. 8(c) elaborates that the star trajectory is larger at the beginning of the searching process and smaller later on, which is due to the change in the value of  $a$ . Fig. 8(d) and (e) illustrate the curve of the feedback gain  $c$  of the GA-ESC and the GA-ESC with PAA, respectively. It reflects that the value of  $c$  adaptively adjusts according to the estimated gradient, which keeps increasing as the robot moves toward the target source. Fig. 8(f) shows the curve of the perturbation parameter  $a$  of the GA-ESC with PAA. When the current point is far from the source, the value of  $a$  is higher, whereas the value of  $a$  gradually decreases on approaching the source.

Table 1 demonstrates that under the same conditions, the average searching time of the GA-ESC and the GA-ESC with PAA to reach the target source is shorter than that of the traditional ESC. Hence, the proposed algorithms can perform well in the diffusion-dominated environment.

#### 4.2. Simulation in the advection-diffusion model

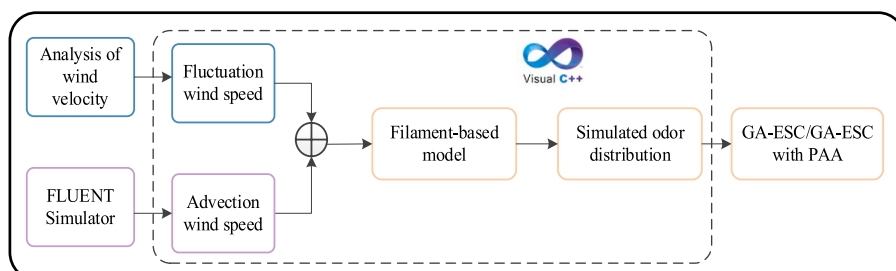
The odor concentration distribution is shown in Eq. (2). The simulation parameters of the dispersion model were chosen as follows: the odor source was set to  $(0, 0)$  m,  $k = 10$ ,  $Q = 1$ , and  $U = 60$ .

Fig. 9 shows an example of the simulation results of each algorithm in the advection-diffusion model. The traditional ESC searching trajectories with feedback gain  $c = 100$  and  $c = 500$  are presented in Fig. 9(a) and (b), respectively. The diagrams reveal that when  $c = 100$ , the robot

**Table 1**

Comparison of the efficiencies of three ESC-based search algorithms in the symmetric quadratic signal field.

Algorithms	Simulation parameters	Average searching time
Traditional ESC with ( $c = 4$ )	$h = 0.1, \Omega = \omega/5, a = 0.1, \omega = 100\pi$	1971
GA-ESC	$h = 0.1, \Omega = \omega/5, M = 900, a = 0.1, \omega = 100\pi$	1646
GA-ESC with PAA	$h = 0.1, \Omega = \omega/5, M = 50, a_0 = 0.5, \omega = 100\pi, \varepsilon = 1, \delta = 0.995$	1639



**Fig. 7.** Indoor filament-based model simulation structure.

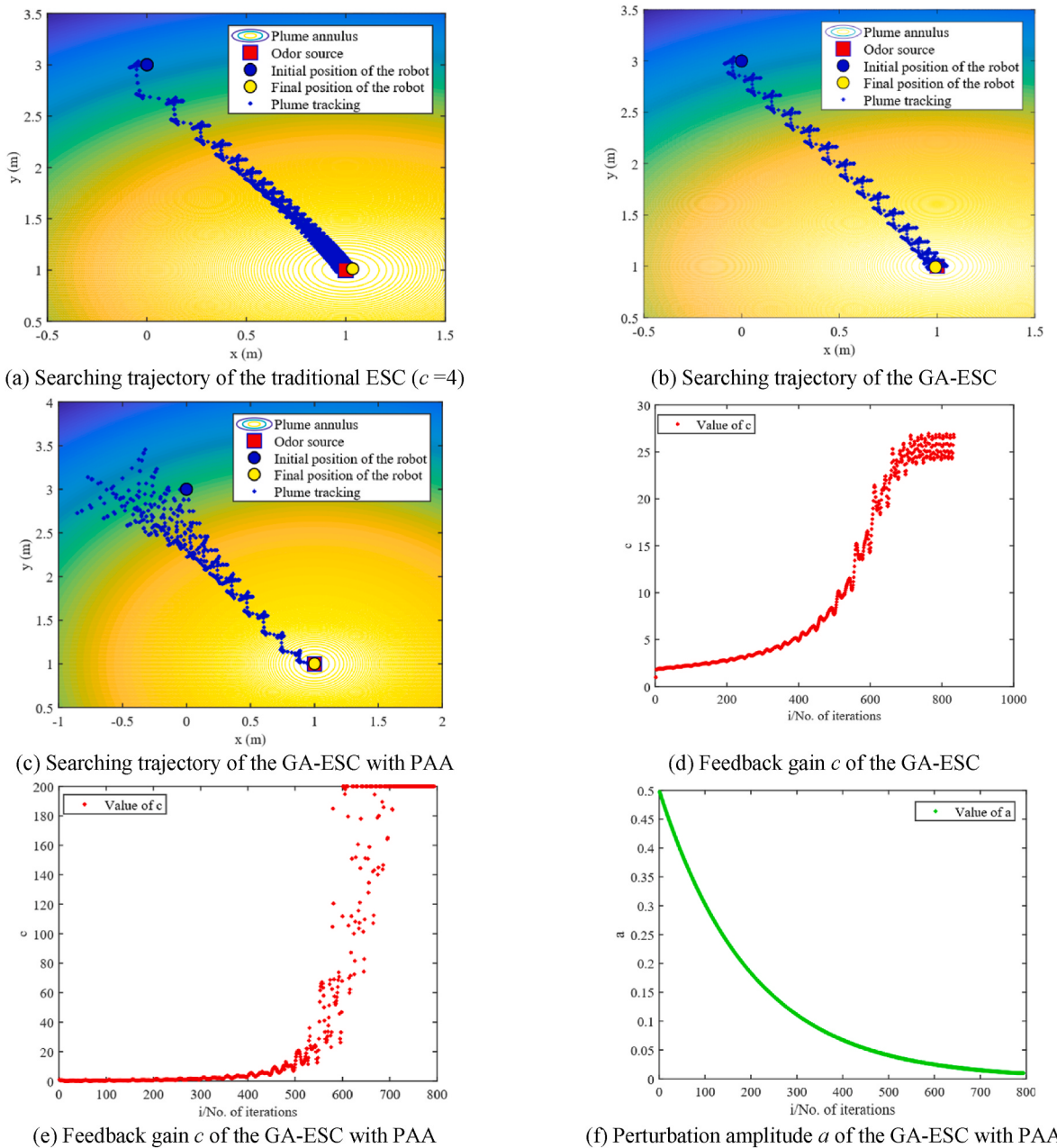


**Fig. 8.** Simulation comparison in the symmetric quadratic model.

remains stuck around the initial position. However, as the value of feedback  $c$  increases (i.e.,  $c = 500$ ), the robot attempts to approach the source but diverges and oscillates in the signal field close to the source. Hence, the traditional ESC could not perform well in the advection-diffusion environment.

Fig. 9(c) and (d) demonstrate that the GA-ESC and the GA-ESC with PAA successfully converge to the optimum point. Fig. 9(e) and (f) illustrate the curve of feedback gain  $c$  of the GA-ESC, and the GA-ESC with PAA, respectively. The feedback gain decreases with an increase in the concentration gradient. During the first 200 iterations, the value of  $c$  is continually adjusted from the initial value to the most suitable value due to the effect of the low pass filter. Hence, the convergence rate of the searching trajectory is not consistent for a period after the starting point. After getting a suitable feedback gain value, the trajectory becomes stable, and the robot gradually approaches the source (Fig. 9(d)). Fig. 9(g) shows the adjustment process of the perturbation amplitude  $a$ . The value of  $a$  gradually decreases as the robot approaches the desired

source.

Table 2 demonstrate that the traditional ESC searching process fails to reach the source in 30000 iterations. Hence, the traditional ESC with fixed feedback gain is not sophisticated enough to locate the odor source in an advective-dominated environment. In contrast, the GA-ESC and the GA-ESC with PAA have successfully reached the source, and the searching efficiency of the GA-ESC with PAA is slightly higher than that of the GA-ESC (see Table 2). It reflects that the GA-ESC with PAA has strong adaptability in the complex environment.

#### 4.3. Simulation in filament-based model

The simulation environment was a ventilated room with the size of  $(8.2 \times 10)$  m, as shown in Fig. 10. The airflow entered from the door in the lower right corner and flowed out of the window in the upper left corner. The odor source was in the lower right corner of the simulation field. The blue arrow represents the airflow, the direction of the arrow

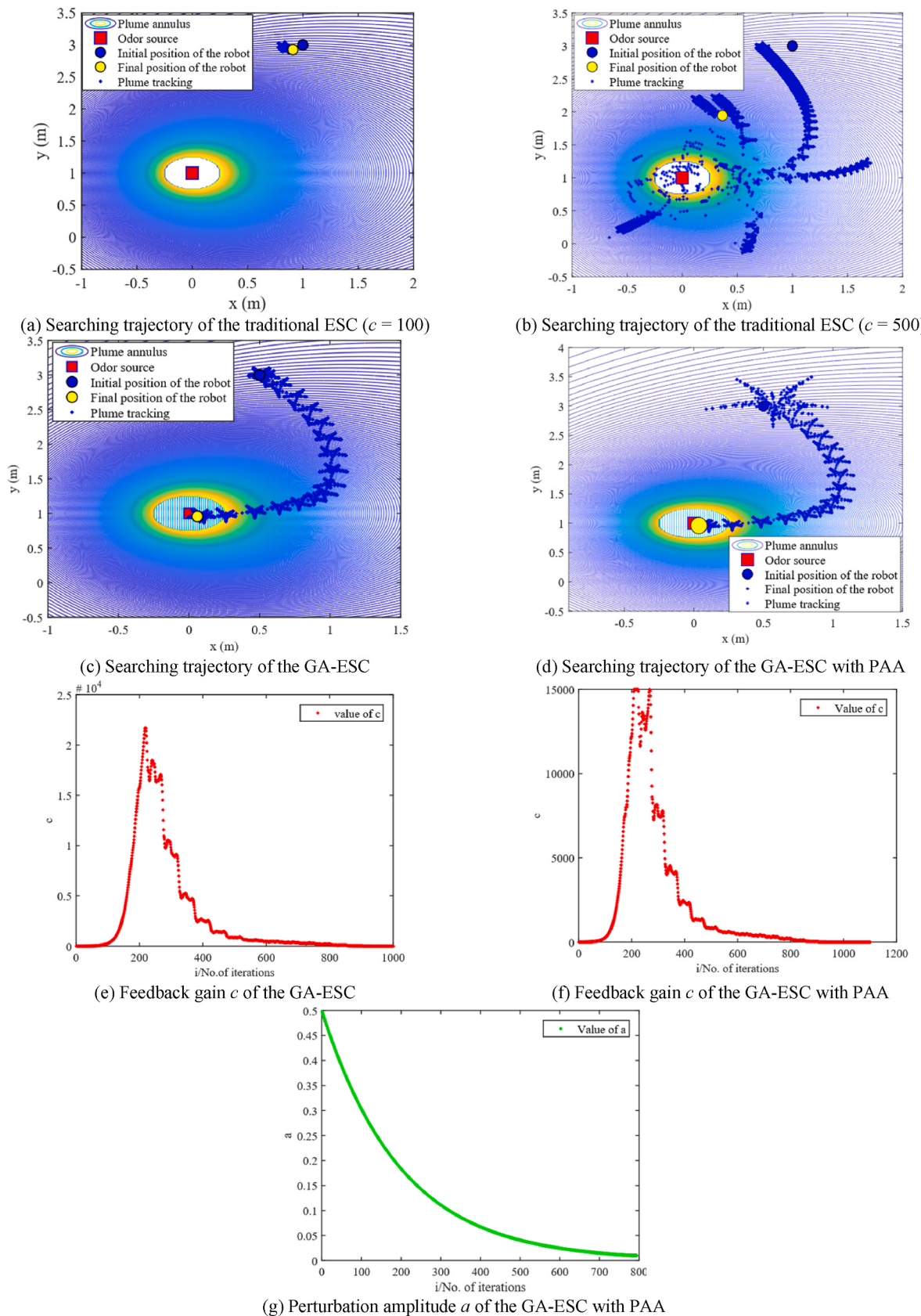


**Fig. 9.** Simulation comparison in the advection-diffusion model.

**Table 2**

Comparison of the efficiencies of three ESC-based search algorithms in the advection-diffusion model.

Algorithms	Simulation parameters	Average searching time
Traditional ESC with ( $c = 500, c = 100$ )	$h = 0.1, \Omega = \omega/5, a = 0.1, \omega = 100 \pi$	>30000
GA-ESC	$h = 0.1, \Omega = \omega/5, M = 900, a = 0.1, \omega = 100 \pi$	1333
GA-ESC with PAA	$h = 0.1, \Omega = \omega/5, M = 50, a_0 = 0.5, \omega = 100 \pi, \epsilon = 1, \delta = 0.995$	1051

describes the wind direction, and the length of the arrow indicates the wind speed. Circular red spots represent the simulated puffs produced by the odor source; the darker the red spot, the higher the concentration. The robot is denoted by a black circle located at the upper left corner of the simulation field; the initial point of the robot was  $(0.5 \times 7.8)$  m. If the robot reached a distance of 0.5 m to the target source, it was deemed successful. When the searching time exceeded 900 s, the robot declared it a failure. The searching time here refers to the total amount of time the robot spent tracking the odor plume until it was within a certain distance of the odor source.

Section 4.2 reveals that traditional ESC diverges and fluctuates close to the odor source in the advection-diffusion environment and cannot reach the source. The filament-based model possesses more complex plume behavior, which is more challenging for OSL. Therefore, the traditional ESC was not evaluated in the filament-based model. In the filament-based model (i.e., the indoor ventilated environment), the GA-ESC and the GA-ESC with PAA were simulated. The common parameters of both algorithms were chosen as  $h = 0.1, \Omega = \omega/5$ . The parameters of the GA-ESC were  $a = 2$ , and  $M = 100$ , whereas  $a_0 = 5, \epsilon = 1, \delta = 0.005$ , and  $M = 70$  were parameters of GA-ESC with PAA. If the robot cannot collect odor concentration information within 20 s, it is assumed to be out of the plume, and the perturbation amplitude  $a$  returns to its initial value. Otherwise, the robot is believed to reach the plume range, and perturbation amplitude begins to attenuate.

The effectiveness of both GA-ESC and GA-ESC with PAA was evaluated by the success rate and the average time taken to find the odor source. For each algorithm, 20 separate simulations were run. If the search duration was longer than 900 s, the search trail was deemed to have failed. Fig. 11(a) reveals that the success rates of the GA-ESC and GA-ESC with PAA are 80% and 95%, respectively. Fig. 11 (b) and (c) show the average localization time for both algorithms and the robot's

seeking process in the filament-based model, respectively. The average searching time of GA-ESC with PAA is much less than that of GA-ESC. Hence, the adaptive amplitude adjustment helps the algorithm quickly converge to the odor source in a complex environment.

## 5. Experiments in an indoor environment

### 5.1. Experimental setup and mobile robot

In addition to the simulation, the GA-ESC was assessed in an indoor ventilated environment without obstacle blocking. The hardware platform used for the experiment included a two-wheeled mobile robot (Two-wheeled mobile robot (Fig. 12(a)) was developed by the Institute of Robotics and Autonomous Systems of Tianjin University), a high-speed odor plume concentration acquisition module (data acquisition module), and auxiliary modules such as odor source, fan, and camera. A humidifier filled with liquid anhydrous ethanol was used as the gas source. The odor patches were released from the outlet on the top of the humidifier. The source was placed near the door. The camera was deployed in the ceiling of the room to record the experimental trials. A controllable fan was used for steady airflow in the room. The experimental area for the robot was  $(2.4 \times 3.6)$  m (Fig. 12(b)).

The two-wheeled mobile robot was equipped with a robot console, data acquisition module, and motor control module. Moreover, the host computer was used to run GA-ESC, and communicate with the robot. The flow chart of the modules is represented in Fig. 13. The details of each module are described as follows.

- Robot console – The robot console was designed by using the esayarm2131 development board. The main task of the robot console was to initialize all the ports (i.e., a Bluetooth serial port, a motor control chip, and a wireless communication system), and communicate with other modules and the host computer through the RPC2A ultra-high frequency wireless communication module.
- Data acquisition module – During mobility, the robot needs to perform numerous activities, i.e., receiving control commands, motor drives, and wireless communication. It was difficult for the robot controller to transmit the collected gas concentration information at a high rate while continuously receiving control commands. Since the odor distribution in the real environment is dynamic and unpredictable, therefore more sensitive and high-frequency sampling is required to fully comprehend the gas concentration information. In order to solve this issue, the data

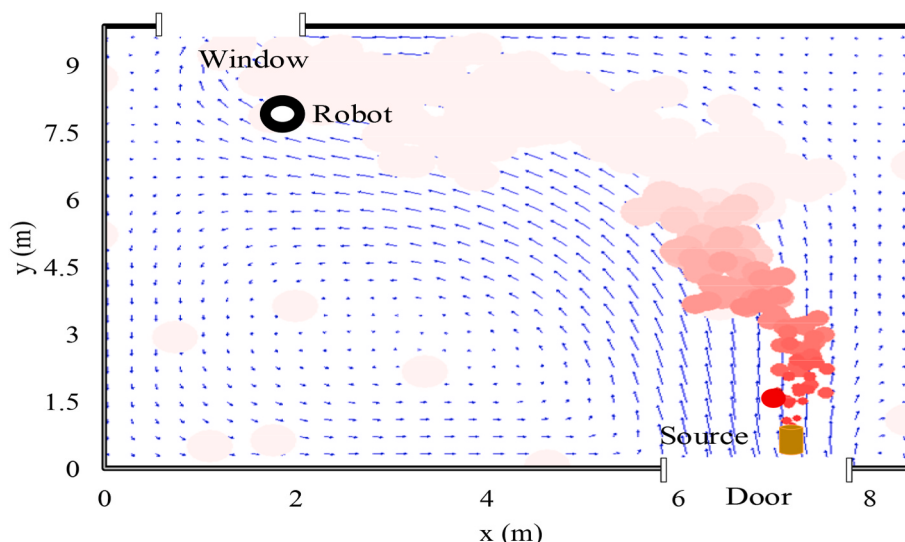


Fig. 10. Simulation environment (simulated plume environment).

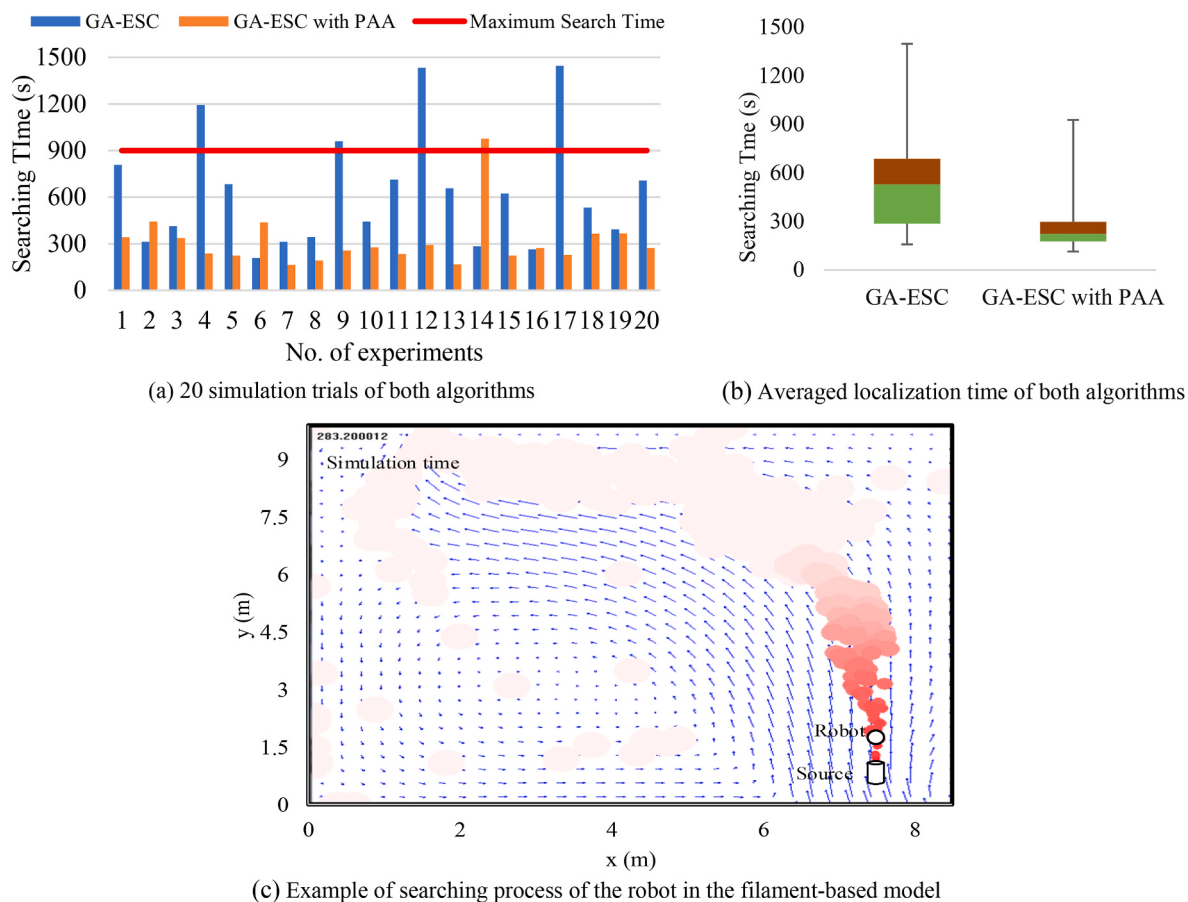


Fig. 11. Locating odor source using GA-ESC and GA-ESC with PAA in the filament-based model.

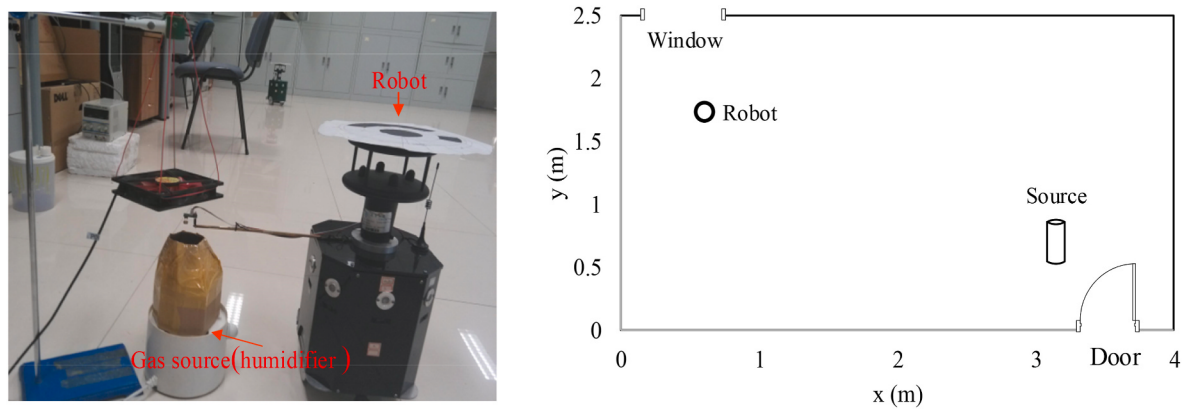


Fig. 12. Experiment setup.

acquisition module was designed to collect high-frequency concentration information. The data acquisition module was composed of an Arduino NanoV3.0 controller, a Bluetooth serial port module, a gas sensor, and a lithium battery. The gas sensor MiCS-5521 (E2V, UK) was deployed to collect the gas concentration information. MiCS-5521 is a metal oxide semiconductor (MOS)-type sensor that is sensitive to volatile organic chemicals, particularly ethanol. This sensor can respond to changes in gas concentration by varying the voltage, i.e., if the detected gas concentration increases, and the

voltage of the sensor increases. The voltage value is filtered and transmitted to the AD (analog-to-digital) sampling pin of the Arduino controller, which exports the acquired data to the host computer via a Bluetooth serial port.

- Motor control module – The motor control module consists of a motion control processor LM269 [38] and motors with encoders. The motor control module (motor actuation) receives the control command from the host computer through the wireless communication module, sets the forward velocity and the angular velocity of the

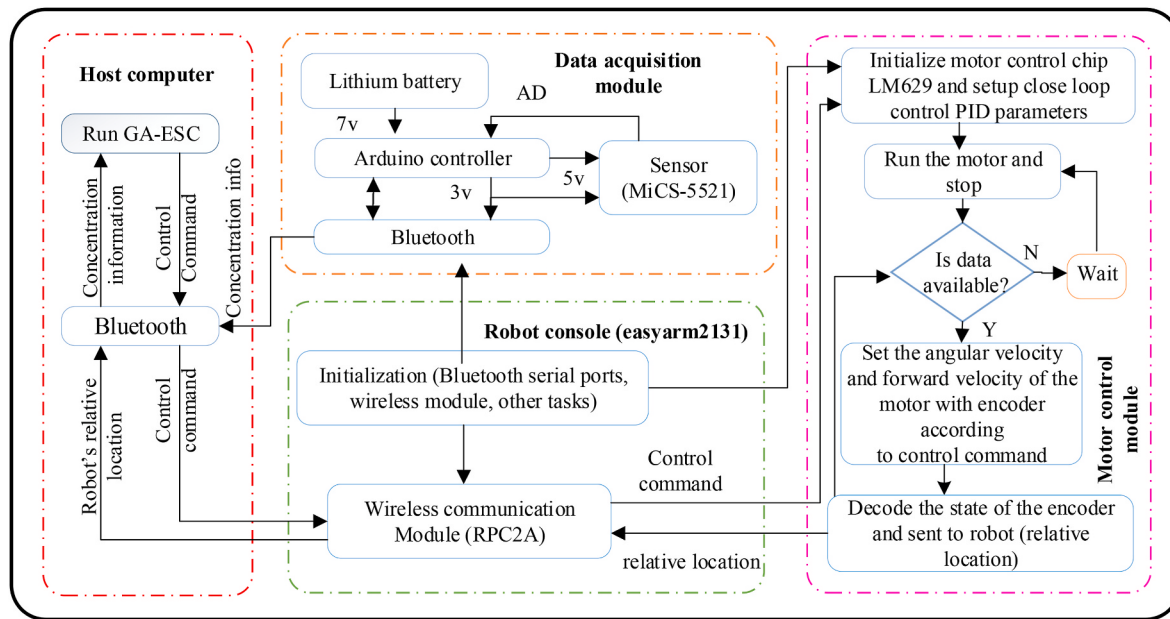


Fig. 13. Flow chart of the experimental setup.

motor according to the control command, and after decoding, sends the robot's relative location back to the host computer.

- Host computer – The host computer receives the concentration information from the data acquisition module. Then the GA-ESC was used to generate the forward velocity and the angular velocity of the mobile robot. Finally, these velocities were converted into the control command format and sent to the robot console via a Bluetooth serial port.

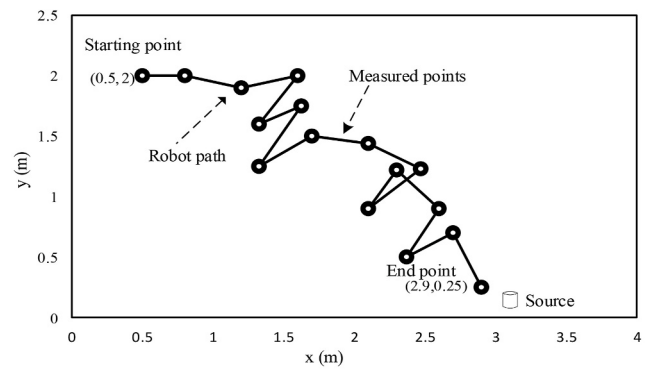
## 5.2. Odor source localization experiment

The data acquisition module was in charge of collecting the sensor's odor plume concentration information from the experimental environment and transmitting it to the host computer via Bluetooth, primarily used to measure the concentration of the odor. Using the gas concentration received from the data acquisition module in the host computer, the GA-ESC determined the velocities and sent control commands to the robot, and the robot moved closer to the source along the direction of the estimated gradient. A total of 15 experimental trials were conducted. We waited a short time before starting the next trial to ensure that the experimental lab was fully clear of the anhydrous ethanol dispersion from the previous trial. A fan was placed behind the odor source to produce steady air flow and simplify the odor flow (near the door). As soon as the gas plume reached the starting point, the robot was started to prevent it from going out of the experimental area. The robot started following the odor concentration when it detected the concentration greater or equal to 4.5 ppm. The robot moved for 3– 4 s and then stopped to estimate the gradient for 8 s. This process was repeated until the robot reached within 20 cm of the odor source, and the experiment was considered successful. It should be mentioned that the searching trial was declared to be successful or unsuccessful manually since we did not apply a source declaration algorithm.

## 5.3. Experimental results and discussion

For the convenience of the experiment, only GA-ESC was evaluated. The GA-ESC with PAA will be examined in a future study. The parameters of the GA-ESC were  $h = 0.02$ ,  $\omega = 100\pi$ ,  $\Omega = \omega/5$ ,  $M = 600$ , and  $a = 35$ . It is worth noting that the values of the experimental parameters differ significantly from the simulated ones due to the random nature of

plume dispersion in realistic airflow environments and the influence of factors such as sensor delays. The performance of the proposed algorithm was evaluated using the searching time and success rate. The mobile robot's starting point was (0.5, 2)m in the downwind direction of the odor source. A set of 15 trials were conducted, 11 trials were successful in finding the odor source, and 4 failed. The average searching time was 120.8 s. For each trial, the robot started at the same location. Each trial's searching time was recorded, and each trial was intended to be completed within 500 s. Fig. 14(a) illustrates one of the odor-searching trajectories of the successful trials. Fig. 14(b) depicts the search time for the 15 trials. The experimental results elucidate that the



(a) Sketch of one of the experimental scenarios  
— Searching time of each trail — Maximum Search Time

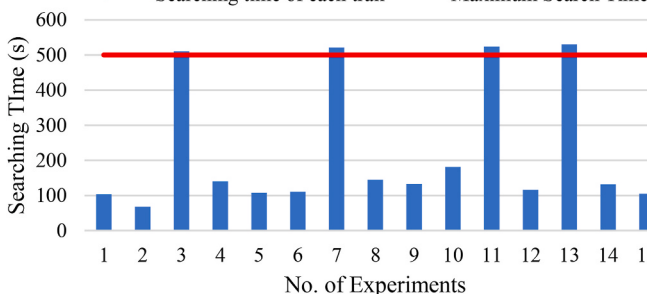


Fig. 14. Experiment in real plume environment.

GA-ESC algorithm can complete the task of OSL with a success rate of 80%.

Some possible causes of 20% failure include: 1) The ESC algorithms use the gas concentration gradient to get the extremum value, while the gas concentration is inconsistent in different experimental times. In the real world, the gradient of gas distribution is chaotic. Convergence of global extremum might be occasionally difficult, although the proposed algorithm can escape local extrema to some extent after adjusting the parameters adaptively. Combining the proposed algorithms with other odor-searching algorithms may produce better results. 2) Furthermore, airflow has a significant impact on the robot as well as plume distribution. Utilizing wind field data to guide the proposed algorithm could enhance the success rate of OSL.

## 6. Conclusions

A GA-ESC algorithm was proposed for odor source localization (OSL), which estimates the gradient of the odor source according to the information of two historical points and the current point. Different from the classic OSL methods, the GA-ESC algorithm solves OSL from the control point of view, and has the advantage of strong stability to perturbations. To enhance the global searching ability of the proposed GA-ESC algorithm, a perturbation amplitude adjustment strategy was introduced, where the amplitude of the perturbation signal decreases with increasing the gradient (i.e., closer to the source). Thus, the larger perturbation signal leads to a more reliable estimated gradient and enabled better global searching ability. Whereas, when getting closer to the source, a smaller perturbation amplitude is helpful for convergence. Moreover, we compared the proposed algorithms with the traditional ESC algorithm in different odor dispersion models via simulations. The results indicate that the GA-ESC and the GA-ESC with PAA algorithm outperform the traditional ESC with a high success rate and less average searching time. The GA-ESC algorithm was also verified in an obstacle-free indoor environment, and the results show that the proposed algorithm successfully approaches the source with a reasonable success rate.

In this study, we have demonstrated the proposed GA-ESC and GA-ESC with PAA algorithms in an obstacle-free environment using a single robot. However, the proposed algorithms could be applied to multiple robots in an environment with obstacle(s), which is the subject of our future work.

## CRediT authorship contribution statement

**Meh Jabeen:** Writing – review & editing, Writing – original draft, Visualization, Validation, Software, Resources, Methodology, Investigation, Formal analysis, Data curation, Conceptualization. **Qing-Hao Meng:** Writing – review & editing, Visualization, Validation, Supervision, Resources, Project administration, Funding acquisition, Conceptualization. **Tao Jing:** Writing – review & editing, Visualization, Validation, Conceptualization. **Hui-Rang Hou:** Writing – review & editing, Visualization, Validation, Funding acquisition, Conceptualization.

## Declaration of competing interest

The authors declare that they have no known competing financial interests or personal relationships that could have appeared to influence the work reported in this paper.

## Data availability

The authors do not have permission to share data.

## Acknowledgment

This work was supported by the National Natural Science Foundation

of China (No. 62203321) and the China Postdoctoral Science Foundation (2021M692390). In addition, the authors would like to thank Mr. Man Yan-Peng for his assistance in simulations and experiments during the research process.

## Appendix A. Supplementary data

Supplementary data to this article can be found online at <https://doi.org/10.1016/j.buildenv.2023.109983>.

## References

- [1] B. Wang, C. Wu, L. Huang, L.B. Zhang, L.G. Kang, K.X. Gao, Prevention and control of major accidents (MAs) and particularly serious accidents (PSAs) in the industrial domain in China: current status, recent efforts and future prospects, Process Saf. Environ. 117 (2018) 254–266.
- [2] L. Zeng, J. Gao, L. Lv, R. Zhang, Y. Chen, X. Zhang, Z. Huang, Z. Zhang, Markov-chain-based inverse modeling to fast localize hazardous gaseous pollutant sources in buildings with ventilation systems, Build. Environ. 169 (2020), 106584.
- [3] Z.Q. Li, Z.F. Tian, T.F. Lu, H.Z. Wang, Assessment of different plume-tracing algorithms for indoor plumes, Build. Environ. 173 (2020), 106746.
- [4] X. Chen, J. Huang, Odor source localization algorithms on mobile robots: a review and future outlook, Robot. Autonom. Syst. 112 (2019) 123–136.
- [5] T. Lewis, K. Bhagangan, A comprehensive review of plume source detection using unmanned vehicles for environmental sensing, Sci. Total Environ. 762 (2021), 144029.
- [6] B. Bayat, N. Crasta, A. Crespi, A.M. Pascoal, A. Ijspeert, Environmental monitoring using autonomous vehicles: a survey of recent searching techniques, Curr. Opin. Biotechnol. 45 (2017) 76–84.
- [7] T. Jing, Q. Meng, H. Ishida, Recent progress and trend of robot odor source localization, IEEJ T. Electr. Electr. 16 (2021) 938–953.
- [8] K. Gaurav, A. Kumar, R. Dayal, Veco-axis as a novel engineered algorithm for odor source localization, Int. J. Ambient Comput. 11 (2020) 1–29.
- [9] K. Mjos, F. Grasso, J. Atema, Antennule use by the american lobster, *homarus americanus*, during chemo-orientation in three turbulent odor plumes, Biol. Bull. 197 (1999) 249–250.
- [10] H. Ishida, K. Hayashi, M. Takakusaki, T. Nakamoto, Odour-source localization system mimicking behaviour of silkworm moth, Sensor Actuat. A-Phys. 51 (1996) 225–230.
- [11] R.A. Russell, A. Bab-Hadiashar, R.L. Shepherd, G.G. Wallace, A comparison of reactive robot chemotaxis algorithms, Robot. Autonom. Syst. 45 (2003) 83–97.
- [12] F. Wario, O. Avalos, J. Gálvez, Chapter 11 - Bio-Inspired Algorithms, Bio-Signal Processing and Classification Using Computational Learning and Intelligence, Academic Press, 2022, pp. 225–248.
- [13] F. Rahbar, A. Marjovi, A. Martinoli, Design and performance evaluation of an algorithm based on source term estimation for odor source localization, Sensors 19 (2019) 656.
- [14] J.G. Li, Q.H. Meng, Y. Wang, M. Zeng, Odor source localization using a mobile robot in outdoor airflow environments with a particle filter algorithm, Aut. Robots 30 (2011) 281–292.
- [15] Y. Ji, Y. Zhao, B. Chen, Z. Zhu, Y. Liu, H. Zhu, S. Qiu, Source searching in unknown obstructed environments through source estimation, target determination, and path planning, Build. Environ. 221 (2022), 109266.
- [16] M. Hutchinson, H. Oh, W.H. Chen, Entrotaxis as a strategy for autonomous search and source reconstruction in turbulent conditions, Inf. Fusion 42 (2018) 179–189.
- [17] M. Vergassola, E. Villermaux, B.I. Shraiman, Infotaxis' as a strategy for searching without gradients, Nature 445 (2007) 406–409, 7126.
- [18] N. Gunawardena, K.K. Leang, E. Pardykaj, Particle swarm optimization for source localization in realistic complex urban environments, Atmos. Environ. 262 (2021), 118636.
- [19] S. Zhou, C. Zhang, H. Cai, B. Zhang, Q. Feng, L. Feng, F. Li, B. Zhou, Locating a time-varying contaminant source in naturally ventilated indoor environments: an experimental study to find effective multi-robot olfaction methods, Build. Environ. 216 (2022), 108954.
- [20] Y. Liu, X. Zhao, J. Xu, S. Zhu, D. Su, Rapid location technology of odor sources by multi-UAV, J. Field Robot. 39 (2022) 600–616.
- [21] Y. Tan, D. Nesić, I.M.Y. Mareels, A. Astolfi, On global extremum seeking in the presence of local extrema, Automatica 45 (2009) 245–251.
- [22] M.A. Ghadiri-Modares, M. Mojiri, H.R.Z. Zangeneh, New schemes for GPS-denied source localization using a non-holonomic unicycle, IEEE Trans. Control Syst. Technol. 25 (2017) 720–727.
- [23] C. Zhang, D. Arnold, N. Ghods, A. Siranosian, M. Krstic, Source seeking with non-holonomic unicycle without position measurement and with tuning of forward velocity, Syst. Control Lett. 56 (2007) 245–252.
- [24] N. Atanasov, J. Le Ny, N. Michael, G.J. Pappas, Stochastic source seeking in complex environments, in: 2012 IEEE International Conference on Robotics and Automation, 2012, pp. 3013–3018.
- [25] M. Ghadiri-Modares, M. Mojiri, Normalized extremum seeking and its application to nonholonomic source localization, IEEE Trans. Autom. Control 66 (2020) 2281–2288.

- [26] M.A. Ghadiri-Modarres, M. Mojiri, H.R.Z. Zangeneh, Nonholonomic source localization in 3D environments without position measurement, *IEEE Trans. Automat. Control* 61 (2016) 3563–3567.
- [27] J. Cochran, M. Krstic, Nonholonomic source seeking with tuning of angular velocity, *IEEE Trans. Automat. Control* 54 (2009) 717–731.
- [28] T. Xu, G. Chen, G. Zhou, Z. Liu, Z. Zhang, S. Yuan, Fast source seeking with obstacle avoidance via extremum seeking control, in: 2021 13th Asian Control Conference (ASCC), IEEE, Jeju, Korea, 2097–2102.
- [29] J. Lin, S. Song, K. You, C. Wu, 3-D velocity regulation for non-holonomic source seeking without position measurement, *IEEE Trans. Control Syst. Technol.* 24 (2015) 711–718.
- [30] S. Xu, Y. Wang, D. Xu, X. Zhu, H. Chen, A review on source seeking control and its application to wheeled mobile robots, in: 2019 3rd Conference on Vehicle Control and Intelligence (CVCI), IEEE, Hefei, China, 2019, pp. 1–5.
- [31] B. Zhou, J. Ke, Z. Han, X. Guan, A review of extremum seeking control or source seeking control and its application of mobile robot, in: 2019 IEEE 9th Annual International Conference on CYBER Technology in Automation, Control, and Intelligent Systems (CYBER), IEEE, Suzhou, China, 2019, pp. 1541–1546.
- [32] S.L. Brunton, J.N. Kutz, Dynamical systems, and control, in: Data-driven Control in Data-Driven Science and Engineering: Machine Learning, Cambridge university press, 2019.
- [33] Y. Tan, D. Nesić, I. Mareels, On non-local stability properties of extremum seeking control, *Automatica* 42 (2006) 889–903.
- [34] H. Ishida, T. Nakamoto, T. Moriizumi, Remote sensing of gas/odor source location and concentration distribution using mobile system, *Sensor Actuat. B-Chem.* 49 (1998) 52–57.
- [35] J.A. Farrell, J. Murlis, X. Long, W. Li, Filament-based atmospheric dispersion model to achieve short time-scale structure of odor plumes, *Environ. Fluid Mech.* 2 (2002) 143–169.
- [36] J. Monroy, V. Hernandez-Bennetts, H. Fan, A. Lilienthal, J. Gonzalez-Jimenez, GADEN: a 3d gas dispersion simulator for mobile robot olfaction in realistic environments, *Sensors* 17 (2017) 1479.
- [37] S. Edelkamp, S. Schrödl, Chapter 17 - vehicle navigation, in: Heuristic Search, Morgan Kaufmann, San Francisco, 2012, pp. 737–757.
- [38] [https://mil.ufl.edu/projects/gnuman/spec\\_sheets/lm628.pdf](https://mil.ufl.edu/projects/gnuman/spec_sheets/lm628.pdf) visited 4th January 2022.